



RESEARCH LETTER

10.1002/2014GL060238

Key Points:

- The 1 April 2014 M_w 8.1 earthquake ruptured about 20% of the 1877 seismic gap
- The rupture was very localized and did not rupture to the trench
- The northern and southern ends of the 1877 gap have now had similar ruptures

Supporting Information:

- Readme
- Figure S1
- Figure S2
- Figure S3
- Figure S4
- Figure S5
- Figure S6
- Figure S7

Correspondence to:

T. Lay,
tlay@ucsc.edu

Citation:

Lay, T., H. Yue, E. E. Brodsky, and C. An (2014), The 1 April 2014 Iquique, Chile, M_w 8.1 earthquake rupture sequence, *Geophys. Res. Lett.*, *41*, 3818–3825, doi:10.1002/2014GL060238.

Received 15 APR 2014

Accepted 21 MAY 2014

Accepted article online 24 MAY 2014

Published online 6 JUN 2014

The 1 April 2014 Iquique, Chile, M_w 8.1 earthquake rupture sequence

Thorne Lay¹, Han Yue¹, Emily E. Brodsky¹, and Chao An²

¹Department of Earth and Planetary Sciences, University of California, Santa Cruz, California, USA, ²School of Civil and Environmental Engineering, Cornell University, Ithaca, New York, USA

Abstract On 1 April 2014, a great (M_w 8.1) interplate thrust earthquake ruptured in the northern portion of the 1877 earthquake seismic gap in northern Chile. The sequence commenced on 16 March 2014 with a magnitude 6.7 thrust event, followed by thrust-faulting aftershocks that migrated northward ~ 40 km over 2 weeks to near the main shock hypocenter. Guided by short-period teleseismic P wave backprojections and inversion of deepwater tsunami wave recordings, a finite-fault inversion of teleseismic P and SH waves using a geometry consistent with long-period seismic waves resolves a spatially compact large-slip (~ 2 – 6.7 m) zone located ~ 30 km downdip and ~ 30 km along-strike south of the hypocenter, downdip of the foreshock sequence. The main shock seismic moment is 1.7×10^{21} N m with a fault dip of 18° , radiated seismic energy of 4.5 – 8.4×10^{16} J, and static stress drop of ~ 2.5 MPa. Most of the 1877 gap remains unbroken and hazardous.

1. Introduction

Northern Chile experienced a great subduction zone megathrust earthquake on 9 May 1877 with an estimated seismic magnitude of 8.7–8.9 [Comte and Pardo, 1991] and a tsunami magnitude M_t of 9.0. Recent geodetic measurements of eastward deformation of the upper plate indicate that most of the 1877 rupture zone (Figure 1) from 19°S to 23°S has a high coupling coefficient, albeit with some patchiness along strike and along dip [e.g., Béjar-Pizarro et al., 2013; Métois et al., 2013]. This region has been identified as the north Chilean seismic gap [Kelleher, 1972; Nishenko, 1985] based on the lack of large earthquakes for the 137 years over which the Nazca plate has been underthrusting South America at about 65 mm/yr [DeMets et al., 2010]. On the order of 6 to 9 m of slip deficit may have accumulated since 1877. The earthquake history prior to 1877 is uncertain [Nishenko, 1985; Comte and Pardo, 1991], so it is unclear whether the region regularly fails in huge single ruptures or intermittently in larger ruptures then sequences of smaller ruptures, as is the case along the Ecuador-Colombia coastline [Kanamori and McNally, 1982]. The rupture zone of the 1868 Peru earthquake, with an estimated seismic magnitude of 8.5–8.8, partly reruptured in the 23 June 2011 M_w 8.4 Peru earthquake (Figure 1), leaving an ~ 100 km long region offshore of southeastern Peru just north of the 1877 gap that may also have large slip deficit [e.g., Loveless et al., 2010].

On 16 March 2014, a M_w 6.7 thrust event occurred on or near the megathrust about 60 km north-northwest of Iquique, Chile, and was followed by two weeks of thrust aftershocks that slowly migrated (~ 20 km/week) northward along the megathrust from 20.2°S to 19.6°S . The location of this sequence in the northern portion of the 1877 seismic gap focused attention on the region, and on 1 April 2014, a M_w 8.1 interplate thrust earthquake initiated at the northern end of the foreshock sequence (19.642°S , 70.817°W , 23:46:46 UTC [U.S. Geological Survey (USGS) National Earthquake Information Center (NEIC): <http://earthquake.usgs.gov/regional/neic/>]). The global centroid moment tensor (gCMT) solution for this event [<http://www.globalcmt.org/CMTsearch.html>] indicates an almost purely double-couple faulting geometry with strike 357° , dip 18° , and rake 109° at a centroid depth of 21.9 km and centroid location south of the hypocenter (19.77°S , 70.98°W), with a centroid time shift of 42.5 s and seismic moment of 1.69×10^{21} N m (M_w 8.1) (Figure 1). A substantial aftershock sequence ensued, the largest of which occurred on 3 April 2014 with M_w 7.7 (02:43:14 UTC, 20.518°S , 70.498°W , centroid depth 31.3 km), 49 km southwest of Iquique. The region extending from updip of the 3 April event southward to $\sim 23^\circ\text{S}$, updip of the 2007 M_w 7.7 Tocopilla earthquake rupture zone [e.g., Béjar-Pizarro et al., 2010; Schurr et al., 2012], remains strained and has potential for either an $\sim M_w$ 8.5 event or several smaller great events (Figure 2).

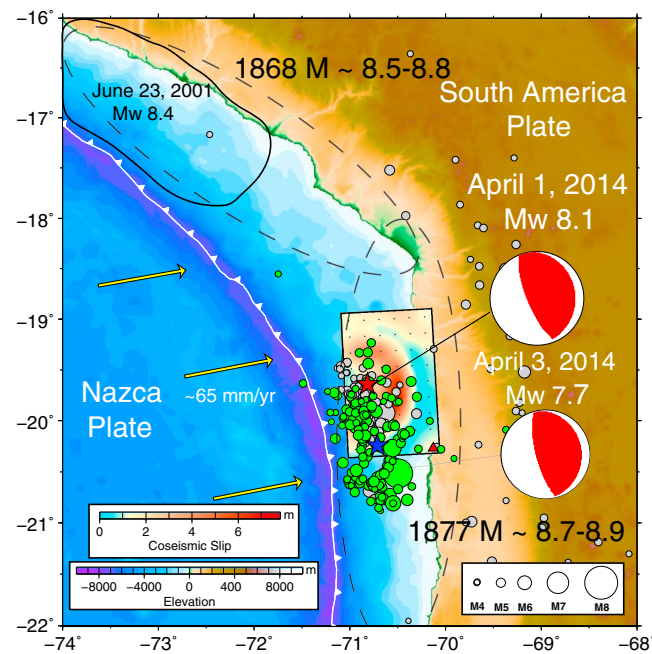


Figure 1. Map of the subduction zone along which the Nazca plate underthrusts South America in southern Peru and northern Chile. The USGS-NEIC epicenter of the 1 April 2014 M_w 8.1 earthquake (red star) and the epicenters of foreshocks from 16 March 2014 to 1 April 2014 (gray circles) and aftershocks from 1 April 2014 to 8 April 2014 (green circles) are shown scaled with symbol size proportional to seismic magnitude. The focal mechanisms are global centroid moment tensor (gCMT) best double-couple solutions for the main shock and the 3 April 2014 M_w 7.7 aftershock. The preferred coseismic slip distribution based on the inversion of teleseismic body waves is contoured in the rectangular plot. The estimated rupture zones of historic large earthquakes in 1868 and 1877 are shown by dashed ellipses. The rupture zone of the 23 June 2001 M_w 8.4 Peru earthquake [Lay *et al.*, 2010] is also shown. The yellow arrows indicate the motion of the Nazca plate relative to a fixed South America plate based on the model MORVEL [DeMets *et al.*, 2010]. The W-phase solution centroid location is indicated by the blue star. The red triangle is the location of GPS station IQQE.

2. Quantifying the 2014 M_w 8.1 Earthquake Sequence

The north Chilean megathrust region from 19°S to 21°S has more frequent large earthquakes in seismological catalogs such as PAGER-CAT [Allen *et al.*, 2009], dating back to 1900 than the adjacent portions of the 1868 and 1877 seismic gaps (Figure 2). Some of these events are likely intraplate based on their rather uncertain locations (Figure S1 in the supporting information). Following the 2001 Peru earthquake, the rate of activity for events with magnitude ≥ 4.5 increased in the vicinity of the 2014 sequence. Focal mechanisms from the gCMT catalog, dating back to 1976, are sparse along the southern portion of the 1868 rupture zone and the 1877 zone other than for the 2014 thrusting sequence (Figure S1 in the supporting information).

A W-phase inversion was performed for the 2014 main shock using 160 ground motion recordings from 112 global seismic stations with stable signals in the period range of 200 to 1000 s. This yielded an almost purely double-couple solution with best double-couple strike 348.7°, dip 14°, and rake 90.7°, with moment of 1.99×10^{21} N m (M_w 8.1), centroid time shift of 45 s, depth of 30.5 km, and location 20.242°S, 70.710°W (Figure 1). This is compatible with the gCMT solution.

Teleseismic P waves from the 2014 main shock, recorded at uniformly spaced North American broadband stations, were aligned by multistation cross-correlation coefficient of the early P wave energy, filtered in the period range of 2.0–0.5 s and then backprojected to the source region following the procedure of Xu *et al.* [2009]. The normalized time-integrated beam power for integrations over 10 s moving windows with time shifts of 1 s is shown in Figure 3 (an animation of the time sequence is shown in Figure S7 in the supporting information). The imaged short-period energy release region is surprisingly concentrated, extending along strike about 100 km, and located below the coastline downdip from the hypocenter, but the absolute location depends on the hypocenter location and can be offset from the actual slip distribution. The foreshock and aftershock sequences locate updip of this short-period source region.

Teleseismic body wave inversions for a large rupture with concentrated slip tend to have strong trade-offs between rupture velocity and spatial extent of slip, due to lack of resolved directivity. We sought to define a priori bounds on the permissible rupture extent using tsunami observations from deepwater pressure sensors of the NOAA and Chilean DART systems. Three high-quality recordings of the main shock tsunami (Figures 4c and 4d) were used. A fault model, based on the megathrust morphology inferred from the trench curvature and regional gravity modeling [Tassara and Echaurren, 2012] that extended to the trench and along strike several degrees (with ~ 40 km spacing along strike and 20–40 km spacing along dip), was used in an

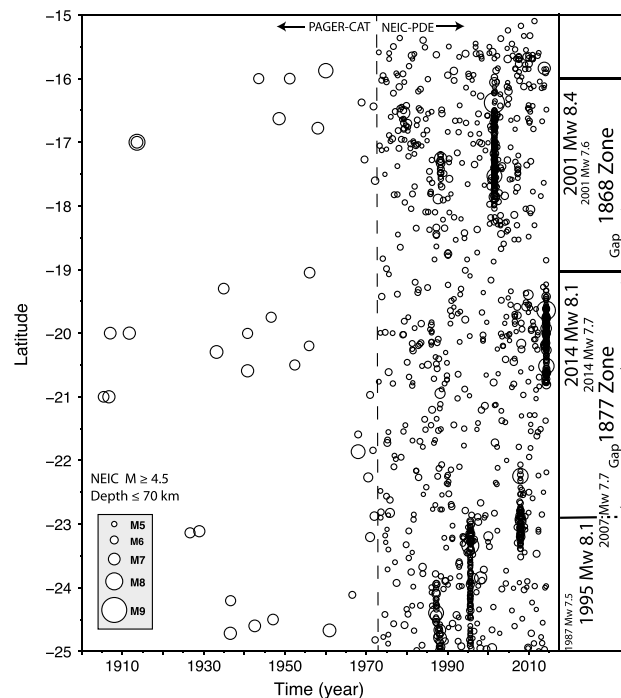


Figure 2. Shallow (depths ≤ 70 km) seismicity from 1900 to 2014 with magnitude ≥ 4.5 from the USGS-NEIC earthquake catalog with pre-1973 events from PAGER-CAT [Allen et al., 2009] located within 200 km from the trench along southern Peru and northern Chile is plotted versus latitude. The detection level of earthquakes varies with time and is much higher prior to 1973. Symbol size is scaled relative to magnitude, and large events are identified on the right, relative to the estimated 1868 and 1877 rupture zones shown in Figure 1. The latitude extent of seismic gaps in the southern portion of the 1877 zone and the overlapping portions of the southern 1868 and northern 1877 zones are indicated by the arrows.

three tsunami recordings, which are given relatively high weight in the joint inversion (a similar model is found by inverting only the tsunami data), suppresses the isochronal expansion of the seismic moment distribution, concentrating rupture in the subfaults near the hypocenter, and allowing inversion without regularization. A very shallow slip near the trench is not consistent with the timing or waveforms of the tsunami, and the overall slip is spatially concentrated downdip of the hypocenter.

Guided by the backprojections and tsunami inversion, we constructed a final preferred finite-fault model from linear least squares inversion of only the seismic data [Kikuchi and Kanamori, 1991]. The rupture model assumes the gCMT strike (357°) and dip (18°) for a planar fault 157.5 km long and 105 km wide with 17.5 km grid spacing (Figure 4e and Figure S2 in the supporting information). The subfault source durations are parameterized with six 2.5 s risetime triangles offset by 2.5 s, giving possible subfault durations of 17.5 s. Rake was allowed to vary for each subfault subevent. Our final seismological model is shown in map view in Figure 1, with a detailed display in Figure 4e. Waveform matches to the P and SH data account for about 88% of the signal power and are shown in Figure S3 in the supporting information. The seismic moment is 1.66×10^{21} N m (M_w 8.08), very close to the gCMT moment. The primary slip zone is about 30 km downdip and 30 km southward along strike from the hypocenter, with slip of up to ~ 6.7 m (peak slip is not a well-resolved parameter) for this model parameterization (Figure 1). The average slip for subfaults with moment at least 15% of the peak subfault moment is 2.6 m, and the static stress drop for a circular fault model with corresponding area is 2.5 MPa. While there is some smearing of the moment distribution along circular isochrons, the imposition of a priori spatial constraints on the inversion leads to very stable results. The centroid time is 41.7 s. There is an ~ 15 s interval of weak teleseismic P wave motion at the onset of this earthquake during which it is unclear whether the rupture expanded or concentrated at the edge of the large

initial inversion. The global seismic data set is composed of 52 P waves and 49 SH wave broadband ground displacements in the period range of 1.1 to 200 s. The same data are used in the inversions of only seismic waves (Figure 4a) and jointly with the tsunami observations (Figure 4b). Subfault rupture durations of 40 s were used for the large grid spacing, which was designed to be compatible with the tsunami wavelength sensitivity. A rupture velocity of 2.2 km/s was assumed. The seismic wave-only inversion, using typical regularization, tends to distribute moment spatially proportional to rupture velocity for the kinematic inversion, even given the long subfault durations, resulting in distributed slip across the fault plane, including extending to near the trench (Figure 4a, Model 1).

Green's functions for the tsunami signals are computed for the model grid using the linear version of the Cornell multigrid coupled tsunami model code, with additional corrections for waveguide and elastic dispersion and water density variations [Tsai et al., 2013] being applied. The bathymetry model had a spatial resolution of 2 arc min, which was resampled from the GEBCO_08 data with a resolution of 30 arcsec. Inclusion of the

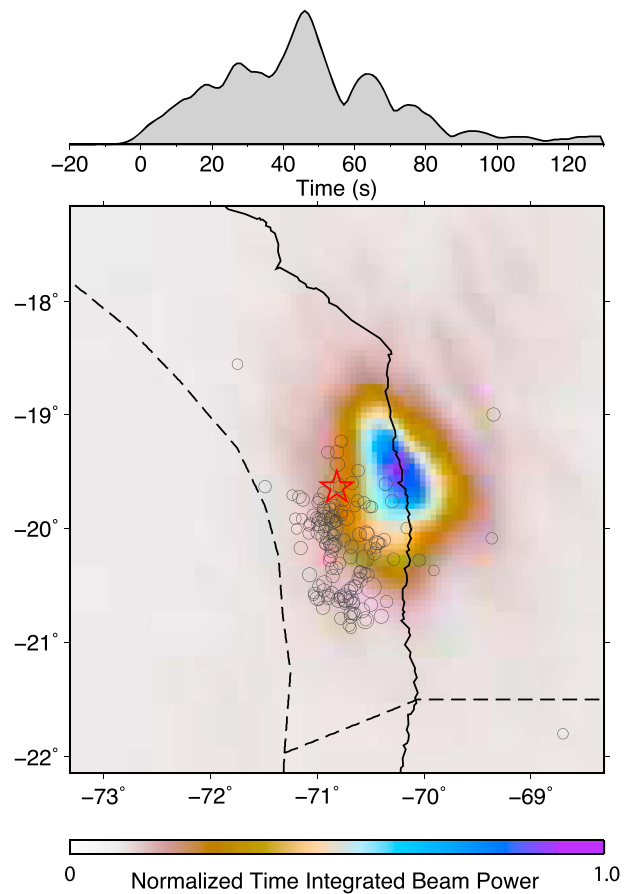


Figure 3. Image of coherent short-period seismic energy release from the 1 April 2014 M_w 8.1 Iquique earthquake, obtained by the back-projection of teleseismic P wave ground displacements in the period range of 0.5 to 2.0 s from North American stations. The time-integrated beam power is shown in the map to display the overall distribution of energy release. The peak beam amplitudes as a function of time is shown at the top. A time-varying sequence of spatial images is provided in Figure S7 in the supporting information.

area is located south of the main shock slip zone, centered near the hypocenter (Figure 1). Our 200 to 600 s period W -phase inversion (based on 114 waveforms from 82 stations) for this event has a moment of 4.47×10^{20} N m, strike 356.6° , dip 16.1° , rake 100.3° , and centroid time shift of 22 s and depth of 35.5 km.

Radiated energy estimates and average source spectra were computed for the 1 April main shock and 3 April aftershock. The total radiated energy for the main shock is estimated to be 8.4×10^{16} J, with a seismic moment-scaled energy ratio of 4.95×10^{-5} . These estimates are based on the average teleseismic P wave spectra for the frequency range of 0.05 to 2.0 Hz for stations with radiation factors larger than 0.5, along with the energy contribution from lower frequencies based on the moment rate spectra for each event (Figure S6 in the supporting information). If we restrict the data to those with radiation factors larger than 0.7, the energy estimate reduces to 6.4×10^{16} J, and if we further restrict to a maximum frequency of 1.0 Hz, it is 4.5×10^{16} J. The source spectrum is generally consistent with a standard interplate frequency-squared reference spectrum with a stress drop parameter of about 3 MPa (Figure S6 in the supporting information). There is no clear indication in the averaged spectra of any slow-slip component associated with the 15 s interval of weak seismic radiation. The 3 April aftershock has a radiated energy of 1.0×10^{16} J, and the seismic moment-scaled energy ratio is 2.3×10^{-5} .

slip patch that ruptured subsequently. Given the imposed kinematic constraints, this model provides a seismological model for the earthquake consistent with very broadband teleseismic observations. This model predicts the ENE direction of ground motion at GPS station Iquique (IQQE) (located in Figure 1) well but overpredicts the offset by 60%.

A finite-fault model based on the teleseismic P and SH wave broadband ground displacements was also developed for the M_w 7.7 aftershock on 3 April 2014. This rupture also has a very concentrated slip distribution. The same strike and dip as for the main shock (which is the same as the gCMT solution for the 3 April event) are used with a hypocentral depth of 35 km and a 9×9 grid with 10 km spacing. A low rupture velocity of 1.75 km/s and moderately long subfault rupture durations composed of seven 2 s risetime triangles (16 s) were assumed to allow the rupture to concentrate spatially as much as indicated by the data. The precise rupture velocity is not resolved. The resulting slip model (Figure S4 in the supporting information) and waveform fits (Figure S5 in the supporting information) account for 80% of the waveform power with a seismic moment of 4.27×10^{20} N m (M_w 7.7) and a centroid time of 21 s. The slip

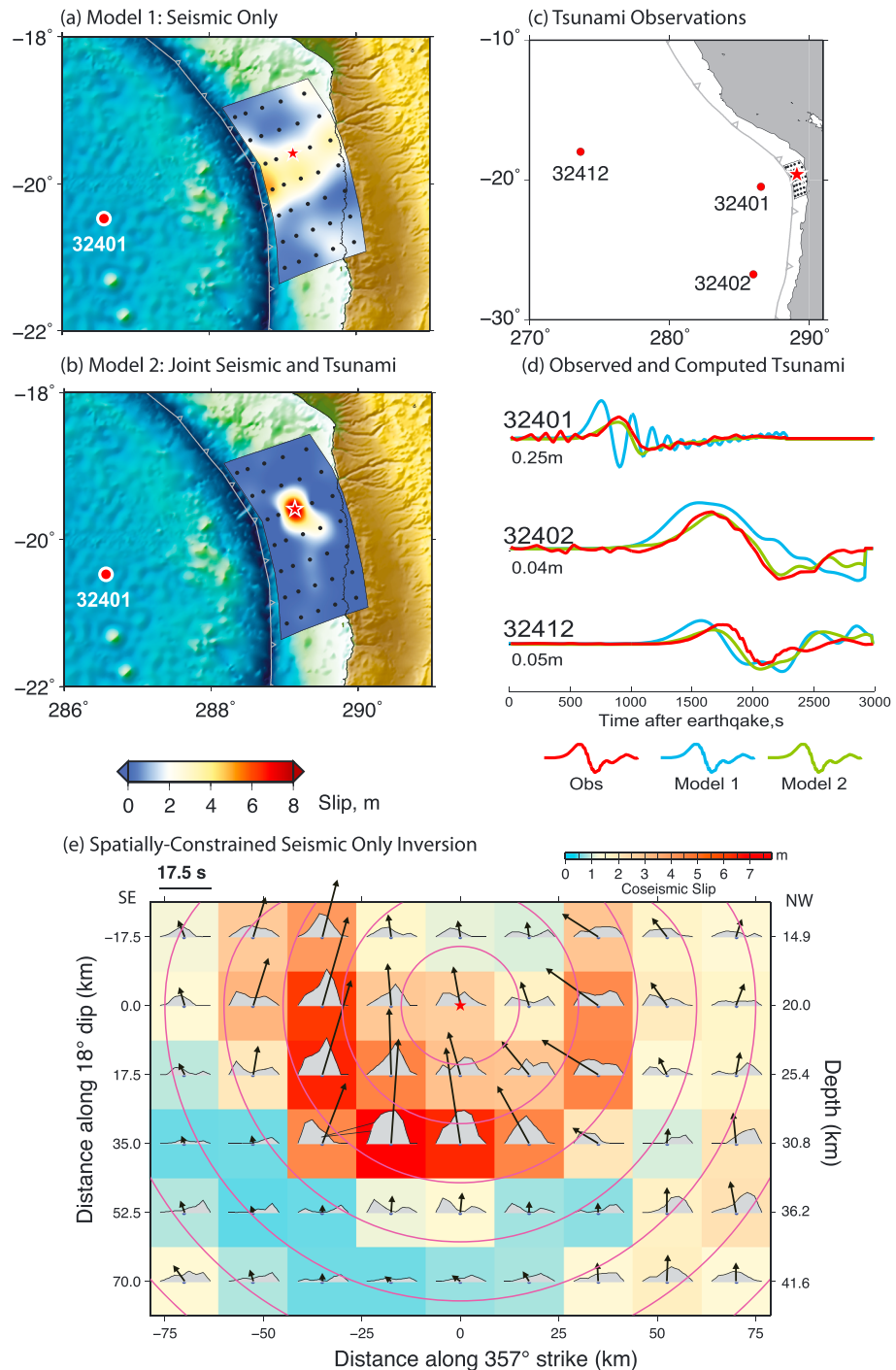


Figure 4. Preliminary and final inversions of teleseismic *P* and *SH* waves and three tsunami sea level observations conducted to establish spatial dimensions of the 1 April 2014 M_w 8.1 rupture. A relatively coarse spatial grid was used, defining subfaults extending all the way to the trench with varying strike, dip, and depth to match the megathrust geometry. (a) Inversion result using only seismic waves in a concentration of slip across the fault plane to the south from the hypocenter. (b) Inversion result using the same seismic data as in Figure 4a joint with (c) three tsunami observations from the locations, with (d) waveforms. The predicted tsunami waveforms for the models in Figures 4a and 4b are compared with the data in Figure 4d, showing that the widely distributed slip some of which extends to the trench is not consistent with the timing, amplitude, or wavelshape of the tsunami signals and that concentrated slip near the hypocenter as in model (Figure 4b) matches the tsunami signals well. (e) The final teleseismic inversion with constrained dimensions of the fault model.

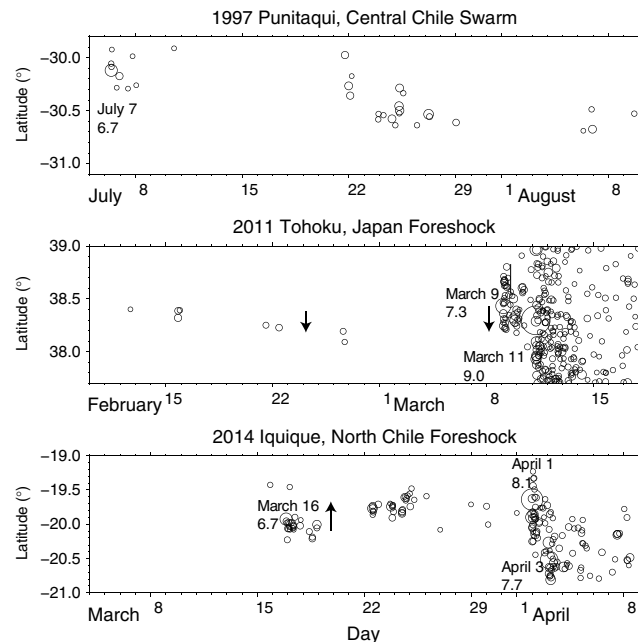


Figure 5. Comparison of three earthquake sequences with magnitudes ≥ 4.5 , involving large interplate thrust faulting in seismic gap regions. (top) The 7 July M_w 6.7 Punitaqui swarm in central Chile along the 1943 earthquake (Coquimbo) seismic gap, (middle) the 2011 Tohoku M_w 9.0 foreshock sequence, and (bottom) the April 2014 Iquique, Chile, sequence.

3. Discussion and Conclusion

The 1 April 2014 M_w 8.1 Iquique earthquake ruptured about 20% of the seismic gap along the larger 1877 rupture. The remaining unbroken zone has now been bracketed by M_w 8.1 events to the north and south (the 1 April 2014 Iquique and 30 July 1995 Antofagasta [e.g., Pritchard *et al.*, 2002] events in Figure 2) and by M_w 7.7 events somewhat downdip on the northern and southern edges of the gap (the 4 April 2014 Iquique and 14 November 2007 Tocopilla events). Geodetic inversions for recent slip deficit suggest relatively uniform coupling in the unbroken region, so failure in a single event is certainly plausible, but the possibility of several smaller events releasing the strain cannot be ruled out. There is little sediment or bathymetric structure on the subducting plate along the remaining gap [Loveless *et al.*, 2010].

The 2014 foreshock sequence is compared in Figure 5 with the foreshock sequence for the great 2011 Tohoku earthquake and a comparable size swarm in 1997 along central Chile that did not lead to a great earthquake. Is it viable to recognize a foreshock sequence like that in 2014 as a definite precursor to an imminent large event or not? A significant number of large interplate events appear to have had foreshock activity and possibly slow-slip events over variable time periods before the large earthquakes [e.g., Bouchon *et al.*, 2013], and it has been suggested that this could assist in earthquake mitigation.

Statistical attributes of the foreshock sequences may reveal anomalous rate increases if prior seismicity is well cataloged. The 2014 foreshock sequence does have unusually high rate increase and has several relatively large events after the magnitude 6.7 event that enhance the regional rate change. The 2011 Tohoku foreshock sequence does not have such a distinctive rate change in teleseismic catalogs, but detailed studies of local recordings reveal an immense number of events in the 2 days between the 9 March 2011 M_w 7.3 foreshock and the main shock [Kato *et al.*, 2012; Marsan and Enescu, 2012]. Migrations of seismicity toward the main shock epicenter at a few kilometers per day occurred in the month preceding the 11 March event and in the 15 to 18 h after the 7.3 foreshock (Figure 5), which has some parallels to the observed northward migration of aftershocks toward the 2014 Iquique main shock hypocenter in the preceding 2 weeks. These migrations tend to support the notion of some slow-slip process concentrating stress near the main shock hypocenter within weeks of the main shock. The 2014 event differs from 2011 in not having sufficient downdip slip to drive rupture updip to the trench. It is not clear if the shallow megathrust in northern Chile is

seismogenic or not, and land-based slip-deficit estimates from geodesy lack resolution near the trench. If the remaining 1877 gap ruptures in a single event, it may drive slip shallower than the 1 April 2014 event. The very large tsunami in 1877 may be indicative of that type of broadening of the slip zone, as occurred in the 2011 Tohoku and 1906 Ecuador-Colombia events.

The July 1997 earthquake sequence in central Chile, near the Coquimbo seismic gap, has a comparable largest event (6.7) to the Iquique foreshocks, and some spatial migration [Gardi *et al.*, 2006; Holtkamp *et al.*, 2011], but was followed by the 15 October 1997 M_w 7.1 Punitaqui intraslab earthquake (normal faulting ~70 km deep) rather than a great interplate rupture [Pardo *et al.*, 2002]. This megathrust last failed in an M_5 7.9 event in 1943, and prior to that possibly in 1880 [Beck *et al.*, 1998], suggesting that a relatively large strain accumulation is possible. However, geodetic estimates of recent slip deficit in the Coquimbo gap region [Vigny *et al.*, 2009; Métois *et al.*, 2012] are low, so the central Chile region may not be as close to its failure limit, leading to a swarm in a locally modestly coupled region that does not precipitate a larger failure. For the 2014 Iquique events, Béjar-Pizarro *et al.* [2013] and Métois *et al.* [2013] indicate stronger coupling on the deeper portion of the megathrust and less coupling updip near the Iquique events, consistent with the slowly migrating updip foreshock sequence followed by the deeper downdip main shock. Holtkamp and Brudzinski [2011] examined many megathrust earthquake swarms around Pacific subduction zones, finding that they tend to concentrate in regions of low interplate coupling or on the margins of large slip zones. Improved onshore and offshore geodetic and seismic networks in many regions are needed to establish the role of slow-slip events in foreshock sequences and better confidence in advance identification of likely foreshock sequences prior to great interplate events.

Acknowledgments

The IRIS DMS data center was used to access the seismic data from Global Seismic Network and Federation of Digital Seismic Network stations. This work was supported by NSF grant EAR1245717 (T.L.).

The Editor thanks two anonymous reviewers for their assistance in evaluating this paper.

References

- Allen, T. I., K. D. Marano, P. S. Earle, and D. J. Wald (2009), PAGER-CAT: A composite earthquake catalog for calibrating global fatality models, *Seismol. Res. Lett.*, *80*, 57–62, doi:10.1785/gssrl.80.1.57.
- Beck, S., S. Barrientos, E. Kausel, and M. Reyes (1998), Source characteristics of historic earthquakes along the central Chile subduction zone, *J. South Am. Earth Sci.*, *11*, 115–129.
- Béjar-Pizarro, M., *et al.* (2010), Asperities and barriers on the seismogenic zone in North Chile: state-of-the-art after the 2007 M_w 7.7 Tocopilla earthquake inferred by GPS and InSAR data, *Geophys. J. Int.*, *183*, 390–406.
- Béjar-Pizarro, M., A. Socquet, R. Armijo, D. Carrizo, J. Genrich, and M. Simons (2013), Andean structural control on interseismic coupling in the North Chile subduction zone, *Nat. Geosci.*, *6*, 462–467, doi:10.1038/NGEO1802.
- Bouchon, M., V. Durand, D. Marsan, H. Karabulut, and J. Schmittbuhl (2013), The long precursory phase of most large interplate earthquakes, *Nat. Geosci.*, *6*, 299–302.
- Comte, D., and M. Pardo (1991), Reappraisal of great historical earthquakes in the northern Chile and southern Peru seismic gaps, *Nat. Hazards*, *4*(1), 23–44, doi:10.1007/BF00126557.
- DeMets, C., R. G. Gordon, and D. F. Argus (2010), Geologically current plate motions, *Geophys. J. Int.*, *181*, 1–80, doi:10.1111/j.1365-246X.2009.04491.x.
- Gardi, A., A. Lemoine, R. Madariaga, and J. Campos (2006), Modeling of stress transfer in the Coquimbo region of central Chile, *J. Geophys. Res.*, *111*, B04307, doi:10.1029/2004JB003440.
- Holtkamp, S. G., and M. R. Brudzinski (2011), Earthquake swarms in the circum-Pacific subduction zones, *Earth Planet. Sci. Lett.*, *305*, 215–225.
- Holtkamp, S. G., M. E. Pritchard, and R. B. Lohman (2011), Earthquake swarms in South America, *Geophys. J. Int.*, *187*, 128–146, doi:10.1111/j.1365-246X.2011.05137.x.
- Kanamori, H., and K. McNally (1982), Variable rupture mode of the subduction zone along the Ecuador–Colombia coast, *Bull. Seismol. Soc. Am.*, *72*, 1241–1253.
- Kato, A., K. Obara, T. Igarashi, H. Tsuruoka, S. Nakagawa, and N. Hirata (2012), Propagation of slow slip leading up to the 2011 M_w 9.0 Tohoku-Oki earthquake, *Science*, *335*, 705–708.
- Kelleher, J. A. (1972), Rupture zones of large South American earthquakes and some predictions, *J. Geophys. Res.*, *77*, 2087–2103, doi:10.1029/JB077i011p02087.
- Kikuchi, M., and H. Kanamori (1991), Inversion of complex body waves—III, *Bull. Seismol. Soc. Am.*, *81*(6), 2335–2350.
- Lay, T., C. J. Ammon, A. R. Hutko, and H. Kanamori (2010), Effects of kinematic constraints on teleseismic finite-source rupture inversions: Great Peruvian earthquakes of 23 June 2001 and 15 August 2007, *Bull. Seismol. Soc. Am.*, *100*, 969–994, doi:10.1785/0120090274.
- Loveless, J. P., M. E. Pritchard, and N. Kukowski (2010), Testing mechanisms of seismic segmentation with slip distributions from recent earthquakes along the Andean margin, *Tectonophysics*, *495*, 15–33.
- Marsan, D., and B. Enescu (2012), Modeling the foreshock sequence prior to the 2011, M_w 9.0 Tohoku, Japan, earthquake, *J. Geophys. Res.*, *117*, B06316, doi:10.1029/2011JB009039.
- Métois, M., A. Socquet, and C. Vigny (2012), Interseismic coupling, segmentation and mechanical behavior of the central Chile subduction zone, *J. Geophys. Res.*, *117*, B03406, doi:10.1029/2011JB008736.
- Métois, M., A. Socquet, C. Vigny, D. Carrison, S. Peyrat, A. Delorme, E. Maureira, M.-C. Valderas-Bermejo, and I. Ortega (2013), Revisiting the North Chile seismic gap segmentation using GPS-derived interseismic coupling, *Geophys. J. Int.*, *194*, 1283–1294, doi:10.1093/gji/ggt183.
- Nishenko, S. P. (1985), Seismic potential for large and great interplate earthquakes along the Chilean and southern Peruvian margins of South America: a quantitative reappraisal, *J. Geophys. Res.*, *90*, 3589–3615, doi:10.1029/JB090iB05p03589.
- Pardo, M., D. Comte, T. Monfret, R. Boroschek, and M. Astroza (2002), The October 15, 1997 Punitaqui earthquake ($M_w = 7.1$): a destructive event within the subducting Nazca plate in central Chile, *Tectonophysics*, *345*, 199–210.
- Pritchard, M. E., M. Simons, P. A. Rosen, S. Hensley, and F. H. Webb (2002), Co-seismic slip from the 1995 July 30 $M_w = 8.1$ Antofagasta, Chile earthquakes as constrained by InSAR and GPS observations, *Geophys. J. Int.*, *150*, 362–376, doi:10.1046/j.1365-246X.2002.01661.x.

- Schurr, B., G. Asch, M. Rosenau, R. Wang, O. Oncken, S. Barrientos, P. Salazar, and J.-P. Vilotte (2012), The 2007 M7.7 Tocopilla northern Chile earthquake sequence: Implications for along-strike and downdip rupture segmentation and megathrust frictional behavior, *J. Geophys. Res.*, *117*, B05305, doi:10.1029/2011JB009030.
- Tassara, A., and A. Echaurren (2012), Anatomy of the Andean subduction zone: three-dimensional density model upgraded and compared against global-scale models, *Geophys. J. Int.*, *189*(1), 161–168.
- Tsai, V. C., J.-P. Ampuero, H. Kanamori, and D. J. Stevenson (2013), Estimating the effect of Earth elasticity and variable water density on tsunami speeds, *Geophys. Res. Lett.*, *40*, 492–496, doi:10.1002/grl.50147.
- Vigny, C., A. Rudloff, J.-C. Ruegg, R. Madariaga, J. Campos, and M. Alvarez (2009), Upper plate deformation measured by GPS in the Coquimbo gap, Chile, *Phys. Earth Planet. Inter.*, *175*(1–2), 86–95.
- Xu, Y., K. D. Koper, O. Sufri, L. Zhu, and A. R. Hutko (2009), Rupture imaging of the *Mw* 7.9 12 May 2008 Wenchuan earthquake from back projection of teleseismic *P* waves, *Geochem. Geophys. Geosyst.*, *10*, Q04006, doi:10.1029/2008GC002335.